Available online at www.sciencedirect.com
ScienceDirect
Applied Catalysis B: Environmental 80 (2008) 283–294
APPLIED CATALYSIS B: ENVIRONMENTAL
www.elsevier.com/locate/apcatb

Efficient production of hydrogen from natural gas steam reforming in palladium membrane reactor

Yazhong Chen [a,b], Yuzhong Wang [b], Hengyong Xu [b,*], Guoxing Xiong [b,**]

[a] State Key Laboratory of Materials-oriented Chemical Engineering, Nanjing University of Technology, No. 5 Xin Mofan Road, Nanjing 210009, PR China
[b] Dalian Institute of Chemical Physics, Chinese Academy of Sciences, P.O. Box 110, Dalian 116023, PR China

Received 5 February 2007; received in revised form 11 October 2007; accepted 12 October 2007

Abstract

Ultra-thin, high performance composite palladium membrane, developed via a novel electroless plating method, was applied to construct a membrane reactor for methane steam reforming reaction, which was investigated under the following working conditions: temperature 723–823 K, pressure 300–900 kPa, gas hourly space velocity (GHSV) 4000–8000 mL g_{cat}^{-1} h^{-1}, steam-to-carbon feed ratio (S/C, mol/mol) 2.5–3.5 and sweep ratio (defined as the ratio between flux of sweep gas to that of methane at the inlet of catalyst bed) 0–4.3. In contrast with previous investigations using commercial catalysts activated at lower temperatures, the catalyst applied in this work was a nickel-based one pre-reduced at 1023 K. The results indicated that selective removal of H_2 from reaction zone obtained methane conversion much higher than thermodynamic control ones and CO selectivity significantly lower than thermodynamic control values. For instance, 98.8% methane conversion, over 97.0% selectivity to CO_2 and over 95.0% H_2 recovery rate could be obtained under mild working conditions. The much higher performance of membrane reactor was attributed to the combination of hydrogen ultra-permeable Pd-based membrane, highly active catalyst for methane steam reforming with countercurrent sweep gas flux design. Further work on stability investigation may develop an efficient onsite route of hydrogen production for application to proton exchange membrane fuel cells.

Keywords: Hydrogen production; Methane steam reforming; Palladium membrane reactor; Nickel-based catalyst

1. Introduction

Hydrogen production from various fuel sources, particularly biomass-derived fuels through steam reforming, partial oxidation and aqueous phase reforming, etc. [1–10], has been the focus of investigation world wide. For the traditional natural gas (methane) steam reforming (MSR), which is currently carried out using multi-tubular fixed bed reactors to produce syngas (a mixture of H_2 and CO) or H_2. Renewed interesting in MSR has been increasing, due to the fact that improvement on MSR process promisingly offers lower cost of H_2 for PEMFC application. During MSR, the following reversible reactions occur.

$$CH_4 + H_2O = CO + 3H_2, \quad \Delta H^0_{298} = 206\,kJ/mol \tag{1}$$

$$CO + H_2O = CO_2 + H_2, \quad \Delta H^0_{298} = -41\,kJ/mol \tag{2}$$

$$CH_4 + 2H_2O = CO_2 + 4H_2, \quad \Delta H^0_{298} = 165\,kJ/mol \tag{3}$$

Because of the high endothermicity of reactions (1) and (3), higher temperature favors forward reactions. Generally, methane conversion over 80.0% could be obtained over 1123 K. To improve energy efficiency, higher reaction pressure is also applied. To efficiently lower reaction temperature and achieve high methane conversion at the same time, equilibria for MSR reaction should be broken, due to the low methane conversion limited by thermodynamics at low temperatures. As the major products in MSR are H_2 and CO_2 at low reaction temperatures, selective removal of CO_2 or H_2 could meet the purpose [11,12]. Calculation performed by setting a residual H_2 ratio in

* Corresponding author. Tel.: +86 411 84581234; fax: +86 411 84581234.
** Corresponding author. Tel.: +86 411 84379182; fax: +86 411 84694447.
E-mail addresses: Xuhy@dicp.ac.cn (H. Xu), gxxiong@dicp.ac.cn (G. Xiong).

0926-3373/$ – see front matter © 2007 Published by Elsevier B.V.
doi:10.1016/j.apcatb.2007.10.024

equilibrium composition of MSR reaction showed that higher methane conversion could be obtained at lower temperatures [13]. For example, methane conversion of 94.0% was predicted when 90.0% of H_2 was removed from reaction zone at 773 K. Therefore, Pd membrane, whose mechanism is based on a H_2 solution-diffusion mechanism on perm-selective film, has been applied to construct membrane reactors to shift thermodynamic equilibrium limited reactions [12–17].

Advantages of membrane reactor over conventional fixed bed reactor (CFBR) for MSR reaction have been recognized, since Oertel et al. first disclosed improved reaction performances in membrane reactor based on a Pd disk of 100 μm [18]. However, due to the low H_2 permeance of membrane, reaction temperatures in the range of 973–1073 K were still necessary to achieve sufficient methane conversion. To improve H_2 permeance of Pd-based membranes, Kikuchi and co-workers [19,20] invented electroless plating method and prepared thin Pd composite membranes on porous glass substrate. This method was further developed and widely investigated, and some high performance Pd membranes were developed [21]. Using Pd composite membrane in MSR reaction, Kikuchi and co-workers [12] obtained methane conversion of 88.0% at 773 K. Shu et al. [13] investigated MSR reaction in membrane reactor using Pd or Pd-Ag/porous stainless steel composite membranes systematically. Higher reaction temperature, S/C or sweep ratio favored methane conversion, while higher reaction pressure may decrease or increase methane conversion, depending upon other operation parameters. Jorgensen et al. [22] investigated MSR in membrane reactor using a 100 μm thick 23 wt.% Pd-Ag membrane tube. Methane conversion of 51% was obtained at 773 K and 600 kPa, and it became 61% at 1000 kPa. Possible coke-free working conditions for MSR in membrane reactor were predicted. Lin et al. [23] investigated effect of incipient removal of H_2 through Pd membrane on methane conversion in MSR by experiment and modeling. They found that L/S (load-to-surface ratio, defined as inlet volumetric flux of methane relative to membrane area ($m^3\ m^{-2}\ h^{-1}$)) and space velocity had great influence on the performances of membrane reactor. Higher space velocity or higher L/S decreased methane conversion. Basile et al. [24] applied a cold-rolled Pd/Ag alloy membrane to construct membrane reactor for MSR. Influences of different kind of sweep gases such as nitrogen, air, steam, CO and O_2 on conversion were reported. By using O_2 sweep gas, methane conversion of 69.0% was obtained at 723 K. Very recently, Tong et al. [25] investigated MSR in membrane reactor using high performance Pd membrane supported on macro-porous stainless steel. Methane conversion of 96.9% and H_2 recovery rate of 90.4% were obtained at 823 K. They also investigated the influence of different kinds of steam reforming catalysts on the performances of membrane reactor [16]. It was found that catalytic performance impacted not only reaction rate but also H_2 flux across Pd membrane, thus separation efficiency of membrane.

Thus, renewed interest in developing catalysts suitable for MSR reaction at low temperatures was boosted. For instance, Matsumura and Nakamori [26] investigated catalytic performances of nickel-based catalysts for MSR at 773 K. Nickel catalyst supported on γ-alumina was not well reduced at 773 K and inactive for MSR. However, the catalyst reduced at 973 K was fairly active, while Ni^0 was partially oxidized during reaction. Among catalysts with similar nickel content, the one supported on zirconia was the most active. Kusakabe et al. [27] investigated nickel and precious metal catalysts supported on Ce-ZrO_2 solid solutions for MSR reaction. Supported Rh catalyst showed best performances among Ni, Pt, Ru and Rh. However, nickel catalysts were still the preferred choice, due to their wide availability and cheapness. Nickel supported on $Ce_{0.15}Zr_{0.85}O_2$ had obvious superiority over that on γ-alumina. Moreover, investigation by Aparicio et al. [28] on methane dry reforming over nickel catalysts in membrane reactor also suggested that $Ce_xZr_{1-x}O_2$ support, instead of γ-alumina, suppressed coke formation and deposition. The lower CO selectivity and decreased coke deposition may be ascribed to the highly mobile oxygen species, possibly generated through a redox cycle of Ce^{4+}/Ce^{3+}. Though impregnated nickel catalysts were not so active in MSR reaction, nickel-alumina based catalysts prepared via coprecipitation had shown high activity for higher hydrocarbons steam reforming or methanation reactions in 1980s [29,30], and these catalysts were still investigated on their application to biomass gasification recently [31]. Ross et al. [32] investigated different nickel/alumina catalysts prepared via coprecipitation or impregnation. Some evidence was found that two types of sites, metallic crystallites and those derived from surface nickel aluminate spinel, may exist on Al_2O_3 supported catalysts, both of which can participate in MSR and associated reactions. While for nickel/alumina catalysts prepared by coprecipitation, the well-dispersed Ni^0 species derived from surface aluminate may possess good activity for MSR. Our previous work showed that Ni/La-Al_2O_3 catalysts, prepared via coprecipitation, had good performances for higher hydrocarbons steam reforming [33]. In the process for preparation nickel/alumina catalysts by coprecipitation, precipitation process and calcination temperature were found to play an important role in determining nickel aluminate formation and its existence state [34].

Currently, although high methane conversion has been previously reported, generally, the reaction gas hourly space velocity (GHSV) was still small. Furthermore, high fluxes of sweep gases were applied. These working conditions were unpractical, for under most cases, pure H_2 was the desired product. But as suggested by Gallucci et al. [24], using steam as sweep gas at low sweep ratios may be a good choice for pure H_2 production due to the easy separation of steam by condensation. Thus, in a practical membrane reactor, it is vitally important to find the bottleneck in membrane reactor. Besides high performance membrane for H_2 separation, catalysts with high activity at temperatures around 773 K were also indispensable. But in previous studies [12–17,22–25,35–38], nickel-based commercial MSR catalysts activated at lower temperatures were applied. As we know, those catalysts were designed for MSR reaction at temperatures as high as 1123 K, their adaptability to MSR in membrane reactor at a much lower reaction temperature are still very unclear and needs further investigation. This work investigated the application of a

nickel-based catalyst pre-reduced at high temperature in membrane reactor for MSR reaction. The catalytic performances in CFBR and performances in membrane reactor were reported.

2. Experimental

2.1. Pd membrane preparation

The composite Pd membrane was prepared via a novel electroless plating method [39]. The porous α-alumina support was supplied by Membrane Science and Technology Research Center of Nanjing University of Technology. According to manufacturer's specifications, the length of α-alumina support was 300 mm, including 250 mm long glaze and 50 mm long porous part. The outer diameter, inner diameter, and nominal pore size of the support tube were 10.0 mm, 6.2 mm and 500 nm, respectively. One end of the support tube was sealed. The open end was applied for the introduction of a sweep gas flux and collection of permeated H_2 and sweep gas, simultaneously. The procedures for Pd composite membrane preparation involved cleaning of the support, modification of the support, followed by successive sensitizing, activation and plating cycles.

2.2. Catalyst preparation and characterizations

The raw materials for catalyst preparation were obtained from Shanghai Reagent (Shanghai China) and used as received. The catalyst was prepared by a coprecipitation–deposition method according to the following procedures. First, $Mg_4(OH)_4(CO_3)_2$ of particle sizes less than 100 μm was suspended in deionized water in a beaker, then metal nitrates and ammonia solution with concentrations about 1.0 mol dm^{-3} were simultaneously introduced into the beaker under moderate stirring. After the precipitation process, the resulted mixture was further aged for about 2.0 h, then filtered, washed with ammonia added deionized water, dried at 383 K for 12.0 h, and then calcined at 1173 K for 4.0 h. The incorporation of lanthanum and magnesium into the nickel-alumina catalyst was found in our work to enhance the catalytic activity as well as the resistance to carbon deposition in the steam reforming of hydrocarbons, which would be reported in another work. Similar effect could be expected in MSR reaction, therefore, we incorporated lanthanum and magnesium into catalyst.

The composition of catalyst was determined by X-ray fluorescence using a Magix-601 element analyzer. The BET specific surface area, pore size distribution and pore volume of the catalyst were characterized by N_2 adsorption at 77 K using Micromeretics ASAP2010P. Prior to adsorption, the sample was degassed at 623 K for 2.0 h to remove physically adsorbed components. The BET surface area was determined from linear portion of BET equation. Pore volume and average pore diameter were calculated by BJH method using the isotherm desorption branch. H_2 temperature programmed reduction (TPR) was conducted on a self-made micro-reactor, gas chromatograph (GC) system. About 40.0 mg sample was heated from room temperature (RT) to 773 K at 10 K min^{-1} in an Ar flow of 30 mL min^{-1} and kept for 30 min. Then the sample was cooled down to RT. Ar was switched to a 5% H_2-Ar flux of 30 mL min^{-1}. Then the sample was heated from RT to about 1273 K at 10 or 20 K min^{-1} and H_2 consumption rate was monitored by online-GC equipped with a TCD. Powder X-ray diffraction (XRD) was used to determine the crystal phases of fresh and utilized catalysts, which was performed on X' Pert Pro (PW 3071, Philips), with a nickel filtered Cu Kα radiation (λ = 0.15418 nm), operation voltage of 40 kV and current of 40 mA. The particle size of Ni^0, or NiO was calculated from the X-ray line broadening measurements.

$$d_{XRD} = \frac{0.89\lambda}{\beta \cos\theta} \quad (4)$$

where, d_{XRD} was the volume average diameter of the crystallite, λ the Cu $K\alpha_1$ wavelength, β the full width at half maximum.

2.3. Methane steam reforming in conventional fixed bed reactor

MSR reactions were investigated in a conventioanal fixed bed reactor made up of stainless steel with an inner diameter of 10.0 mm. High purity gases N_2, H_2, Ar and CH_4 were utilized. 2.0 g catalyst in grain size range of 420–630 μm was used without dilution. Prior to reaction, the catalyst was activated in a 30.0% (v/v) H_2-Ar flux of 50 mL min^{-1} at 1023 K for 3.0 h, details of the reaction and analysis would be described in the next part. The performance of the catalyst were determined at P = 900 kPa and S/C = 3.0 and GHSV in the range of 8000–96,000 mL g_{cat}^{-1} h^{-1}.

Thermodynamic analysis for the steam reforming of methane was performed using HSC chemistry for Windows V.3.02 (Outokumpu software). The considered reactions include methane steam reforming (Eq. (1)) and WGS as described in Eq. (2).

2.4. Hydrogen permeation and methane steam reforming in palladium membrane reactor

The schematic diagram for H_2 permeation, MSR reaction in membrane reactor and analysis system are illustrated in Fig. 1. The Pd membrane tube was located inside the center of a dense stainless steel tube reactor with an inner diameter of 20.0 mm. An annulus chamber between the stainless steel tube and membrane was thus formed and applied for reaction, which also served as the retentate side of the Pd membrane. While the inner volume of the membrane was the permeate side. The reactor was inserted into a heating furnace connected to a temperature controller/programmer. A thermocouple inserted into thermocouple well was placed in the annulus chamber to determine the catalyst bed temperature. For the membrane reactor, the catalyst was pre-reduced at 1023 K for 3.0 h and cooled down to RT gradually. Then, 5.0 g pre-reduced catalyst in the grain size range of 420–630 μm, diluted with silica was packed to achieve a 60.0 mm catalyst bed height, e.g. the catalyst bed was

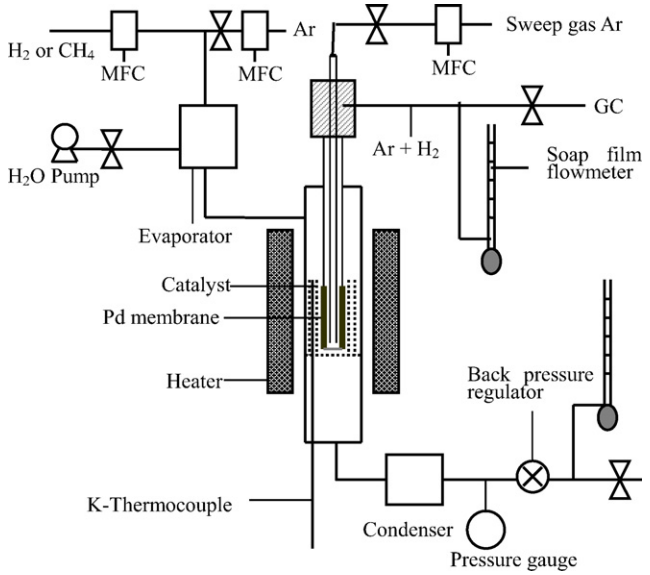

Fig. 1. Schematic diagram of a homemade apparatus for H_2 permeation and methane steam reforming reaction in palladium membrane reactor.

extended 10.0 mm above the position where the membrane separation started. All the feed gases were controlled by mass flow controllers (Brooks Instrument 5850s). Water was delivered to the reactor by high performance liquid chromatograph pump. The pressure of reaction was maintained by a back-pressure regulator connected with a precise pressure gauge to read the pressures. For gas permeation experiments, pure H_2 or N_2 were applied. The permeation flux of H_2, or any leakage were measured at different pressure drops across membrane by a single gas method. Before reaction, the reactor was slowly heated to 723 K at a rate of 2 K min^{-1}, after stabilizing, methane and water was gradually introduced to reactor. The flux in the permeate side, those in reaction side were measured with bubble film gas meters and theoretically calculated according to product selectivities. The concentration of products in reaction side and permeate side were monitored online by Varian CP–3800 gas chromatograph. The calculation of H_2 purity did not take sweep gas argon into account, although inside the permeate chamber argon sweep gas was applied. Methane conversion (X_{CH_4}) was calculated according Eq. (5).

$$X_{CH_4} = \frac{[CO] + [CO_2]}{[CO] + [CO_2] + [CH_4]} \times 100\% \quad (5)$$

H_2 yields were calculated using methane conversion and product selectivities according to Eq. (6).

$$H_2 \text{ yield} = (S_{CO_2} \times 4 + S_{CO} \times 3) \times X_{CH_4} \quad (6)$$

3. Results and discussion

3.1. Catalyst characterization results

The composition of catalyst differed a little with the desired compositions, suggesting that the higher pH value used during coprecipitation–deposition would cause some loss of nickel and aluminum cautions [40]. X-ray fluorescence characterization confirmed that the catalyst had a composition of 31.8 wt.% NiO, 11.8 wt.% MgO, and 2.6 wt.% La_2O_3 and balance alumina, thus the atomic ratio of Ni:Mg:Al:La in the catalyst was 0.43:0.30:1.06:0.015. N_2 adsorption and desorption isotherms at 77 K and pore size distributions are indicated in Fig. 2. Based on the isotherms, the BET surface area was 103.4 m^2 g^{-1}; the high BET surface area obtained even under calcination temperature of 1173 K for 4.0 h may be attributed to the hydrotalcite structures developed during coprecipitation. The pore volume was 0.44 cm^3 g^{-1}, and pore size distribution was in the range of 5.0–20.0 nm.

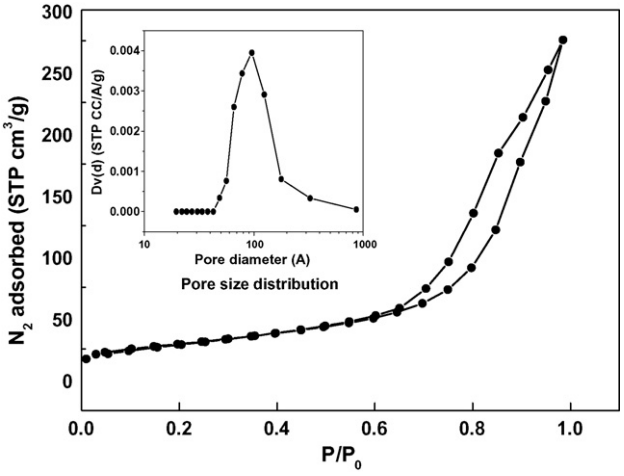

Fig. 2. Nitrogen adsorption isotherm and desorption isotherm measured at 77 K for the fresh catalyst and its pore size distribution.

The XRD patterns of fresh and used catalysts are shown in Fig. 3. Carefully comparing XRD patterns of fresh and used catalysts concluded that both nickel aluminate and magnesium aluminate with spinel structures existed in the fresh catalyst. But due to similarity of reflection peaks for nickel aluminate and magnesium aluminate, strong overlapping of reflection peaks was observed. According to Sloczynski et al. [41], mixed spinel such as $Ni_xMg_{1-x}Al_2O_4$ may be formed, too. Seen from

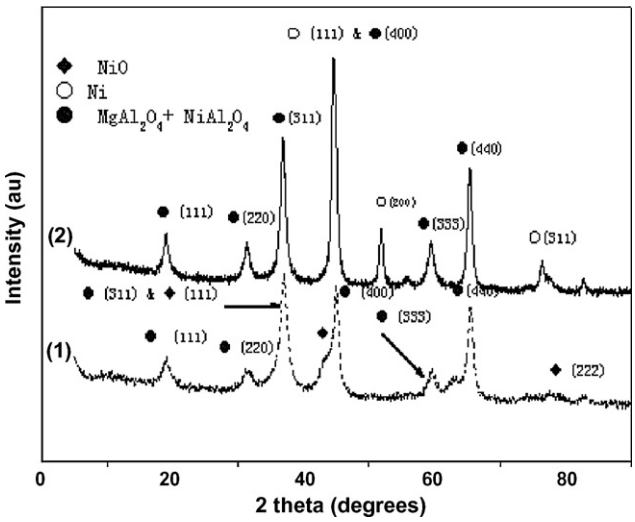

Fig. 3. XRD patterns of fresh catalyst (1) and used catalyst (2).

Fig. 3, NiO reflection peaks were not very obvious in fresh catalyst, due to the overlapping of reflections for NiO and spinel structure, which also suggested that NiO existed in the form mainly as surface nickel aluminate, bulk nickel aluminate or even NiO-MgO solid solution. In the XRD patterns of used catalysts, obvious nickel reflection peaks appeared. The β values for those peaks representing crystal surfaces of aluminate became smaller due to some reduction of nickel aluminate, suggesting that in the fresh catalyst, both spinel structures of nickel aluminate and magnesium aluminate, and even the mixed spinel structure existed. So the main support phase in the catalyst after reduction might be magnesium aluminate. This agreed with results reported by Bangala et al. [42], who used mechanically mixed MgO and Al_2O_3 as support to prepare nickel-base catalyst by impregnation. They found that when calcination temperature was above 1023 K, the magnesium aluminate phase dominated in the support phase.

TPR results (Fig. 4) showed two maxima, one at 1055 K and the other at 1159 K when the temperature ramp rate was 10 K min^{-1}. The peak temperature for the reduction of pure NiO was about 700 K or a little higher [43], depending on the preparation method. In the nickel/alumina catalyst, the reduction peak temperatures were related with the pH values used in precipitation and calcination temperature. Higher pH value and higher calcination temperature shifted TPR peaks to higher temperatures. The first reduction peak shown in Fig. 4 could be ascribed to surface nickel aluminate, possibly existed in the form of solid solution with magnesium aluminate, or an oxide form with strong interaction with alumina and magnesium oxide. The second reduction peak at 1159 K may be ascribed to the formation of stoichiometric nickel aluminate, as suggested by Teixeira and Giudici [44], who found that reduction peak temperature for bulk nickel aluminate of 1140 K in a sample containing 50.0 wt.% Ni, 4.5 wt.% lanthana and balance alumina, prepared by coprecipitation with a calcination temperature of 1173 K. The associated XRD patterns also showed the evidence of these phases. Increase in temperature ramp rate shifted TPR peaks to higher temperatures. For example, the peak temperature corresponding to the possible bulk nickel aluminate shifted from 1159.5 to 1192.4 K when temperature ramp rate increased from 10 to 20 K min^{-1}. Calculation based on reduction peak temperature shifts concluded that apparent activation energy for reduction of surface nickel aluminate was about 129 kJ mol^{-1}, while the other kind of NiO species showed an apparent activation energy for reduction of about 223 kJ mol^{-1}, which may be ascribed to mono-dispersed nickel species [32] among the crystal structure of magnesium aluminate spinel or the stoichiometric nickel aluminate spinel.

3.2. Methane steam reforming in conventional fixed bed reactor

Taking into account the necessity to carry out MSR at a higher pressure to achieve acceptable separation efficiency (defined as the ratio of H_2 flux across membrane (mL min^{-1}) to H_2 production rate (mL min^{-1})) under conditions without a sweep gas, the catalytic performances were tested at 723–823 K, P = 900 kPa, S/C = 3.0 and the results are shown in Fig. 5. It could be seen that in the wide GHSV range, methane conversion close to thermodynamic control ones were obtained. The reaction GHSV was gradually increased until methane conversion showed obvious derivation from thermodynamic control ones. The results in Fig. 5 indicated that at 723 K, in the GHSV range of 8000–64,000 mL g_{cat}^{-1} h^{-1}, experimentally determined methane conversion were very close to thermodynamic control value of 13.1%. Further increase in GHSV to 96,000 mL g_{cat}^{-1} h^{-1} led to methane conversion decrease from 13.1% to 11.7%, but methane conversion experimentally determined at 773 and 823 K in the investigated GHSV range of 8000–96,000 mL g_{cat}^{-1} h^{-1} showed little derivation from the equilibrium values, which were 19.4% at 773 K, and 27.3% at 823 K, respectively. In comparison with recently reported results on MSR reaction at low reaction temperatures, the catalyst showed much higher performances. For instance, Matsumura and Nakamori [26] investigated nickel catalysts supported on various supports. Over 20 wt.% Ni/ZrO_2 catalysts,

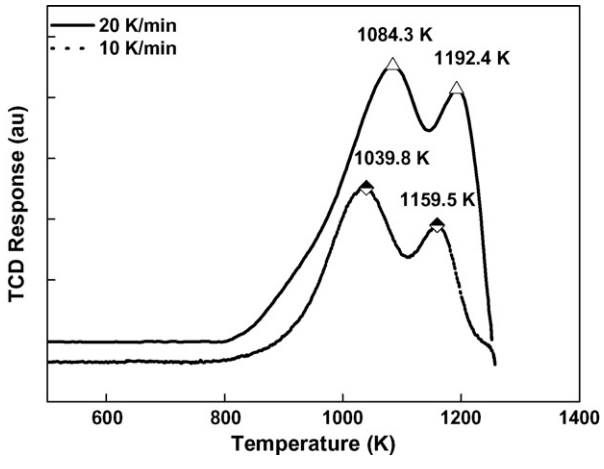

Fig. 4. TPR profiles for the catalyst at different temperature ramp rate in a 5 vol% Ar-H_2 atmosphere.

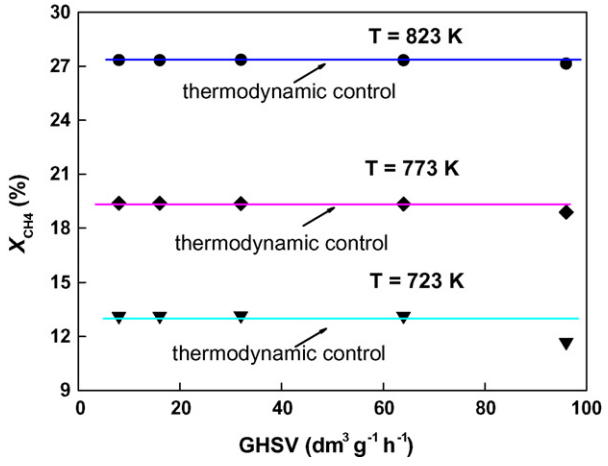

Fig. 5. Influences of gas hourly space velocity on methane conversion at different reactions temperature (reaction conditions: P = 900 kPa and S/C = 3.0).

methane conversion of 25.5% was obtained at $T = 773$ K, $P = 100$ kPa, GHSV = 15,000 mL g_{cat}^{-1} h^{-1} and S/C = 2.0, while the thermodynamic control one under corresponding conditions was 33.8%. Kusakabe et al. [27] recently investigated the catalytic performances of nickel, and precious metals supported on $Ce_xZr_{1-x}O_2$. The catalysts were activated at 773 K, similar with the activation process in membrane reactor. 3.0 wt.% Rh/$Ce_{0.15}Zr_{0.85}O_2$ showed the best performance, and 28.3% methane conversion was achieved at $T = 773$ K, $P = 100$ kPa, GHSV = 27,000 mL g_{cat}^{-1} h^{-1} and S/C = 2.0, which was lower than thermodynamic control one of 33.8%, too. The higher performances of the catalyst may be related with its preparation method, calcination and high temperature reduction. During coprecipitation, hydrotalcite structures, which consisted of Brucite-like layers of compositions $[Ni_xAl_{1-x}(OH)_2]^{(1-x)+}$ and interlayers containing CO_3^{2-}, NO_3^- or OH^- could be developed. In the hydrotalcite structure, the position of Ni^{2+} and Al^{3+} could be taken place by other bivalent, or trivalent cations. This resulted in a close interaction of the species incorporated in the hydrotalcite structure. During our catalyst preparation process, all of metallic ions in catalyst precursors could be incorporated into the hydrotalcite structure theoretically. The average particles size of Ni^0 calculated by line broadening of nickel (2 0 0) reflection peak was 19.1 nm. However, as discussed by Ross et al. [32], the high activity of catalyst may be related with a kind of active sites derived from the surface or bulk nickel aluminate. The surface or bulk nickel aluminate was related to the hydrotalcite structure formation during coprecipitation and calcination. During reduction, due to the strong interaction of alumina with nickel oxide, isolated (mono-dispersed) nickel atoms may be formed according to Eq. (7) [32].

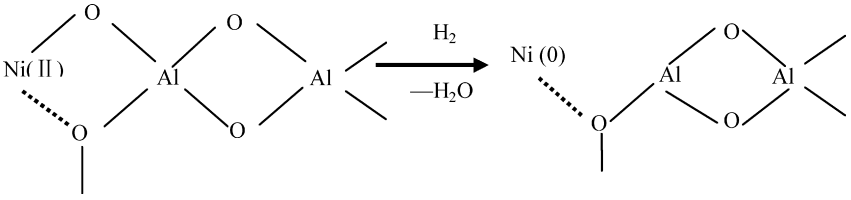

(7)

The resultant nickel Ni(0) still closely associated with alumina structure and their catalytic activity may be closely related with alumina. The formed mono-dispersed nickel site showed different hydrogen adsorption behaviors from that of bulk nickel crystallites and they could possibly participate in MSR as described in the following:

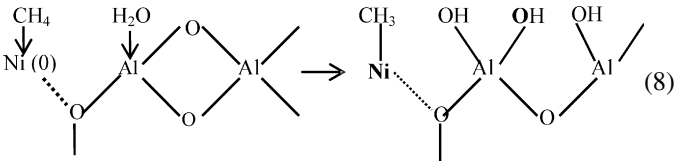

(8)

The CH_3 and OH species subsequently react to give steam reforming products. In our point of view, a higher turnover frequency on active site derived from nickel aluminate than bulk nickel crystallite was expected due to the close proximity of nickel and alumina, or maybe other species like magnesia and lanthana. Both of them had ability to adsorb steam. Provided that the surface reaction of adsorbed carbon species and adsorbed steam was the rate-determining step, the following influences of close proximity of nickel and other oxide species were reasonably deduced. Firstly, it affected the electronic structure of nickel; partial apparent positive electronic charge was predicted in Ni(0) derived from aluminate, which may favor the adsorption of methane. Secondly, it may decrease the surface diffusion path due to close proximity of adsorbed species, thus a higher turnover frequency was predicted. Thirdly, this kind of active sites may show much higher coke deposition resistance due to the fact the interaction between the adsorbed carbon species is difficult to take place. In summary, it is probably that two kinds of nickel species exist in the catalyst, metallic crystallites and sites derived from nickel aluminate, after higher temperature reduction of the catalyst, mono-dispersed nickel may be formed, which may be related with the high MSR activities at lower temperatures. However, no direct evidence for confirmation of the existence mono-dispersed nickel could be provided for the time being, for conventional characterization techniques are incapable in getting such evidence. Thus, further investigation is indispensable to clarify the problem.

3.3. Performances of Pd membrane for H_2 permeation

The H_2 permeance and H_2/N_2 separation coefficient of membrane were determined with pure N_2 and H_2 at 100 kPa pressure drop across the membrane at 773 K. The H_2 permeance of the membrane was 70 m^3 (m^2 bar h)$^{-1}$, while no permeation of nitrogen across the Pd membrane was detected under the same conditions, suggesting an almost infinite H_2 selectivity. The length of the Pd membrane was 50 mm, the membrane area was 15.7 cm^2. The calculated membrane thickness based on weight increase after plating was about 4.0 μm in thickness.

The H_2 permeation behavior under different H_2 partial pressure drops across the membrane and different temperatures were measured using single gas method, too. The permeate side was kept atmospheric pressure. The H_2 permeation flux versus H_2 partial pressure drops across membrane at 773 K was shown in Fig. 6. It suggested that under wide range of pressure drops across membrane, H_2 permeation flux was almost proportional to H_2 partial pressure drops. The exponent value of H_2 partial pressure was about 1.0, showing great derivation from Sievert's law. This indicated that rate-determining step in H_2 permeation across Pd membrane was H_2 dissociative adsorption on Pd surface rather than the bulk diffusion, due to the fact that Pd

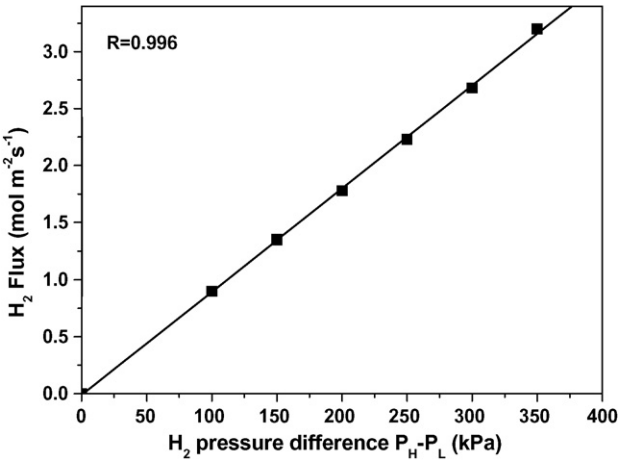

Fig. 6. H_2 permeation flux versus hydrogen partial pressure drops across Pd membrane at 773 K.

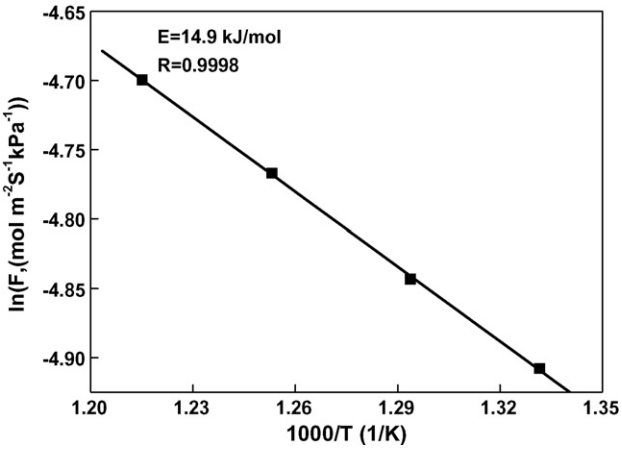

Fig. 7. Arrhenius plot for the Pd/Al_2O_3 composite membrane at H_2 partial pressure difference of 100 kPa within 723–823 K.

membrane was only about 4.0 μm thick [25]. Furthermore, not only increase in H_2 permeation flux with increasing H_2 partial pressure drop across membrane, but also a H_2 flux of 0.86 mol m^{-2} s^{-1} at $T = 773$ K and 100 kPa H_2 partial pressure difference were obtained. The nitrogen permeation flux under similar conditions was found to be almost zero, suggesting that the H_2/N_2 separation coefficient was almost infinite. Comparison with literature results are listed in Table 1, which suggested that Pd membrane had very high performance for H_2 permeation and separation.

The influence of separation temperature on H_2 permeation flux of the membrane is shown in Fig. 7. The good linearity of the curve indicated that under test temperature range, there was no change of rate-determining steps for H_2 permeation. From this Arrhenius plot, apparent activation energy of 14.9 kJ mol^{-1} for H_2 permeation across the membrane was estimated, which agreed with well the results previously reported [24].

3.4. Methane steam reforming in palladium membrane reactor

3.4.1. Influences of the reaction temperature

The major advantage of membrane reactor was conversion enhancement of an equilibrium-limited reaction by selective removal of products. In the case of MSR reaction, membrane reactor can lead to significantly enhanced methane conversion at a lower temperature. However, when reaction temperature was below 673 K, the reforming reaction could not reach a satisfactory conversion level due to the relative low reaction kinetics of MSR, and thermodynamic equilibrium may not be reached. While removal of H_2 through Pd membrane could only slightly shift reforming equilibrium due to the intrinsically favorable temperature influences over 973 K, and high temperature may destroy the Pd membrane, too. Thus, reaction temperature in the range of 723–873 K was usually applied. In such a temperature range, membrane separate H_2 efficiently and higher methane conversion in membrane reactor could be obtained. As shown in Fig. 8, methane conversion in membrane reactor was significantly increased by 260–400% compared with equilibrium values. For instance, under working conditions of $P = 900$ kPa, GHSV = 4000 mL g_{cat}^{-1} h^{-1}, S/C = 3.0 and $I = 2.6$, methane conversion was 65.0% at 723 K, while the equilibrium one was only 13.2%. Within 723–823 K, increase in reaction temperature monotonically increased methane conversion. This was ascribed to the fact that higher temperature favor MSR reaction kinetics as well as H_2 permeation, which resulted in higher separation efficiency. But

Table 1
H_2 Separation efficiency of composite Pd membrane and comparison with literature results

Membrane	Pre method	Thickness (μm)	T (K)	DF (kPa)	H_2 flux (mol m^{-2} s^{-1})	Sepn factor
Pd/MPSS [45]	ELP/O	10	753	100	0.089	1000
Pd/MPSS [46]	ELP	19–28	773	100	0.015–0.023	<5000
Pd/MPSS [47]	ELP	5	673	100	0.155	100
Pd/PG [20]	ELP	13	773	202	0.189	∞
Pd/Al_2O_3 [47]	ELP	7–15	673	100	0.086–0.134	100–1000
Pd/HF [21]	ELP	3–4	703	100	0.136	1000
Pd/Al_2O_3 [48]	CVD	0.5	623	100	0.05	500
Pd-Ag/PG [20]	EFP	21.6	673	202	0.067	∞
Pd-Ag [24]	CR	50	773	100	0.01	∞
Pd/MPSS [25]	MDELP	6.0	773	100	0.26	∞
This work	MELP	~4.0	773	100	0.86	∞

ELP: electroless plating, MPSS: macroporous stainless steel, PG: porous glass, HF: hollow fiber, DF: permeation driving force, CR: cold rolling, MDLEP: multi-dimension electroless plating, MELP: mofified electroless plating.

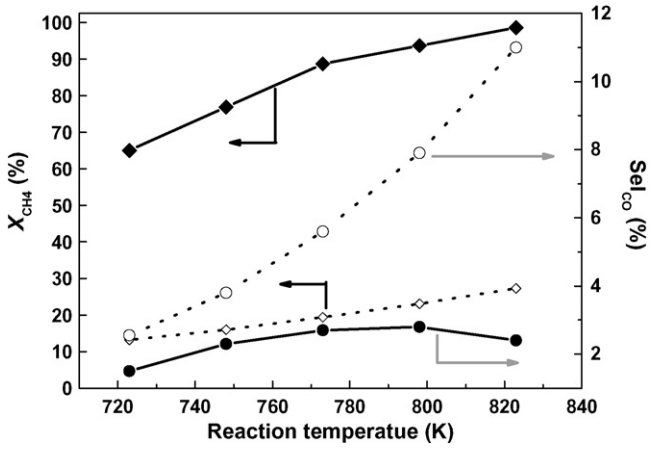

Fig. 8. Influences of reaction temperature on methane conversion and CO selectivity in membrane reactor and equilibrium ones (◆, experimental methane conversion; ◇, equilibrium methane conversion; ●, experimental CO selectivity; ○, equilibrium CO selectivity, reaction conditions: P = 900 kPa, GHSV = 4000 mL g_{cat}^{-1} h^{-1}, S/C = 3.0 and I = 2.6).

impact of temperature became not as pronounced as that at lower temperatures. At 773 K, methane conversion was 88.7%, increase in temperature from 723 to 773 K led to methane conversion increase by 23.7%, while methane conversion increased by only about 10% when the reaction temperature was further increased from 773 to 823 K. As we know, performance of Pd membrane was determined by at least by three interrelated factors: (1) MSR reaction kinetics; (2) H_2 separation efficiency; (3) radial diffusion of H_2 from reaction location to Pd membrane surface in the reaction side. By the combination of highly active steam reforming catalyst, high performance Pd membrane, and a special sweep gas design, methane conversion of 98.8%, and 95.4% H_2 recovery rate was achieved under mild working conditions (T = 823 K, P = 900 kPa, GHSV = 4000 mL g_{cat}^{-1} h^{-1}, S/C = 3.0 and I = 2.6), which was about 93.7% of maximum theoretical H_2 yield. Besides the enhanced methane conversion, CO formation was efficiently suppressed, too. As we know, H_2 selective removal also shifted reaction (2) to the right side. So, a non-monotonic dependence of CO selectivity upon reaction temperature was observed within 723–823 K, e.g. CO selectivity first increased with reaction temperature within 723–773 K, and then showed a slight decrease within 773–823 K. But they were much lower than thermodynamic equilibrium ones. For instance, an experimental CO selectivity of 2.7% was observed at 773 K, while the equilibrium one was 5.6%. At 773 and 798 K, the CO selectivity was almost the same. Then increase in reaction temperatures led to a slight CO selectivity decline, which was shown clearly in Fig. 8. The CO formation was suppressed, which was more pronounced when the reaction temperature was high within 723–823 K. At 723 K, CO selectivity was reduced by 41% compared with the equilibrium one; while CO selectivity was reduced from 11.0 to 2.4% by 69.1% at 823 K. Increase in reaction temperature also gradually enhanced the recovery rate of hydrogen, for instance, at 723 K, recovery rate of hydrogen was 89.0%, it increased to 95.4% at 823 K.

3.4.2. Influences of reaction pressure

In a CFBR, increase in reaction pressure would result in decreased methane conversion, and lower CO selectivity due to the impact of the thermodynamic equilibrium for MSR. However, in membrane reactor, this trend may be changed. Although a higher reaction pressure is unfavorable for methane conversion at thermodynamic equilibrium, the increase in reaction pressures may lead to a higher H_2 partial pressure in the reaction side in membrane reactor, which increases the driving force for H_2 permeation and enhanced H_2 separation efficiency, higher methane conversion under certain conditions could be expected. For example, Tong et al. [25] disclosed that the influence of reaction pressure on methane conversion was related with the reaction GHSV at 100–300 kPa. At lower GHSV, an increase in pressures resulted in a higher methane conversion. While at a higher GHSV of 2000 mL g_{cat}^{-1} h^{-1}, a slight decrease of methane conversion was observed. In our previous work on higher hydrocarbons steam reforming in Pd membrane reactor, in the pressure range of 200–400 kPa, an increase of selectivity to methane was also found when reactions were carried out at T = 823 K, S/C = 2.7 and I = 0 [49], suggesting increasing reaction pressure was unfavorable for methane conversion under these working conditions. The simulation results reported by Gallucci et al. [38] also revealed that, for a membrane-aided reaction system, an increase of reaction pressure corresponds to either an increase or to a decrease in methane conversion, depending on the combination of pressure, temperature, membrane thickness and reactor length. In our point of view, only when H_2 separation efficiency improvement predominated over thermodynamic equilibrium effect, an increase in methane conversion was predicted when reaction pressure increased. The influences of pressure on methane conversion in this work were investigated at T = 773 K, GHSV = 4000 mL g_{cat}^{-1} h^{-1}, S/C = 3.0 and I = 2.6 and the results are shown in Fig. 9. Increase in reaction pressure from 300 to 900 kPa resulted in a monotonic methane conversion enhancement from 67.6 to 88.7%, while the equilibrium controlled methane conversion were predicted to

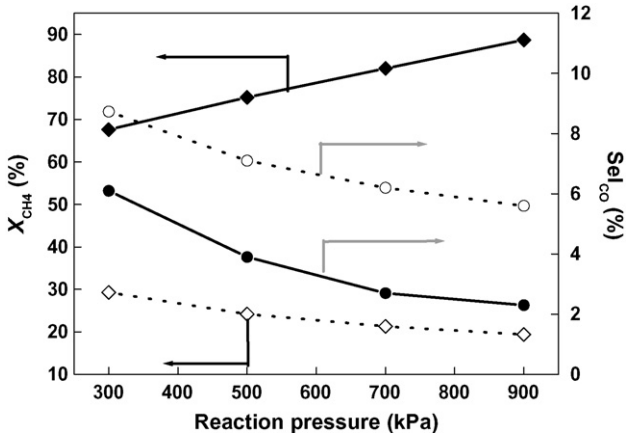

Fig. 9. Influence of reaction pressure on methane conversion, CO selectivity and equilibrium ones (◆, experimental methane conversion; ◇, equilibrium methane conversion; ●, experimental CO selectivity; ○, equilibrium CO selectivity, reaction conditions: T = 773 K, GHSV = 4000 mL g_{cat}^{-1} h^{-1}, S/C = 3.0 and I = 2.6).

decrease from 29.3 to 19.4%. This agreed with results previously reported by Uemiya et al. [2] and Prokopiev et al. [4], e.g. methane conversion increased upon reaction pressure. In our work, higher reaction pressure also suppressed CO formation more efficiently. For example, at 773 K and 300 kPa, CO selectivity was 6.1%; while at reaction pressure of 900 kPa, it was only 2.3%. In contrast with thermodynamic control ones, the trend that CO selectivity decreased with increasing reaction pressure was also observed, but CO reduction by 30–60% was obtained, and this effect was more obvious at higher pressures. Due to the ultra-thin property of the palladium membrane, increase in reaction pressure at $T = 773$ K, GHSV = 4000 mL g_{cat}^{-1} h^{-1}, S/C = 3.0 and $I = 2.6$ monotonically enhanced the recovery rate of hydrogen from 71.0% at 300 kPa to 91.8% at 900 kPa. Thus, the influence of reaction pressure upon methane conversion was a compromise between the influence of thermodynamic equilibrium, and the H_2 separation efficiency which functions oppositely. The monotonic increase of methane conversion with reaction pressure in this work indicates that, the separation efficiency of the Pd membrane is sufficiently high to dominate the performance of Pd membrane reactor under those conditions. Although in the membrane reactor for MSR, reaction pressures as high as 900 kPa was applied, the membrane also showed almost infinite H_2 selectivity under the severe working conditions because no CO_2 or CH_4 was detected in the permeate side.

3.4.3. Influences of reaction gas hourly space velocity

The influences of reaction GHSV on methane conversion and selectivity to CO are illustrated in Fig. 10. A comparison between methane conversion in membrane reactor and those in CFBR was also made. As expected, methane conversion in CFBR was almost unchanged, and close to thermodynamic control value irrespective of reaction GHSV, suggesting the catalyst had sufficient activity for MSR reaction at $T = 823$ K, $P = 900$ kPa and S/C = 3.0. While in Pd membrane reactor, a monotonic decrease of methane conversion with increasing reaction GHSV was observed. Methane conversion decreased from 98.6 to 86.0%, when reaction GHSV increased from 4000 to 8000 mL g_{cat}^{-1} h^{-1}. These results could be related with some interrelated factors. Higher reaction GHSV increased the L/S for the Pd membrane and a shorter residence time, thus a shorter time for the H_2 produced in the reaction to diffuse from the reaction location to membrane surface. On L/S influences, Lin et al. [23] predicted a decreased methane conversion with increasing L/S in the range of 0.1–10.0 m^3 h^{-1} m^{-2}, when the reaction was carried out at WHSV (weight hourly space velocity) less than 1.0 h^{-1}, $T = 773$ K, $P = 900$ kPa or 2000 kPa and $I = 0$. Highest methane conversion of 85.8% was achieved under reaction conditions $T = 773$ K, $P = 2000$ kPa, WHSV = 0.3 h^{-1}, L/S = 0.3 m^3 h^{-1} m^{-2} and $I = 0$. In our work, at $T = 823$ K, GHSV = 4000 mL g_{cat}^{-1} h^{-1}, S/C = 3.0, L/S = 3.5 m^3 h^{-1} m^{-2} and $I = 2.6$, methane conversion of 98.6% was obtained. And increase in GHSV from 4000 to 8000 mL g_{cat}^{-1} h^{-1} only caused a limited methane conversion decrease from 98.6 to 86.0%, which are much better than the results predicted by Lin et al. [23]. The variation in GHSV has no effects on thermodynamic control CO selectivity, but in membrane reactor, the higher GHSV, the higher CO selectivity was observed. For instance, the CO selectivity was only 2.4% at GHSV = 4000 mL g_{cat}^{-1} h^{-1} and 6.3% at GHSV of 8000, while the equilibrium one was 11.0%. Increase in GHSV leads to lower recovery rate of hydrogen. For instance, under the investigated working conditions, recovery rate of hydrogen was 95.4% at GHSV = 4000 mL g_{cat}^{-1} h^{-1}, it decreased to 90.1% and 85.0% at GHSV = 6000, 8000 mL g_{cat}^{-1} h^{-1}, respectively. Besides the effects of reaction kinetics, another physical process – radial mixing diffusion of H_2 from the reaction location to the Pd membrane surface in a packed-bed type of Pd membrane reactor would also impact the membrane separation efficiency, and this process was closely related to the residence time. Itoh et al. [50] found that calculation based on ideal flow model would give higher separation efficiency than calculation results based on radial diffusion model. Thus, it could be assumed that when the permeance of the Pd was sufficiently high and the kinetics of the catalyst fast enough, performances of the membrane reactor would be determined by neither the kinetics of catalyst nor the H_2 permeation across the Pd membrane, instead, the physical process, radial diffusion of H_2 from reaction location to Pd membrane surface, may determine the performances of membrane reactor. However, this could be solved by using hollow fiber membranes or capillary membrane module to shorten the diffusion path [21]. Under our reaction conditions, as the catalyst applied was highly active, and the Pd membrane could permeate H_2 through fast enough, we ascribed the moderate decrease of methane conversion, largely to the influences of radial diffusion time shortening, which are to be confirmed by modeling. Of course, other effects such as concentration polarization would also result in a lower separation efficiency which was inevitable in gas mixture separation [51]. When reaction GHSV increased, H_2 flux across membrane also increased, thus the concentration polarization effects are more severe.

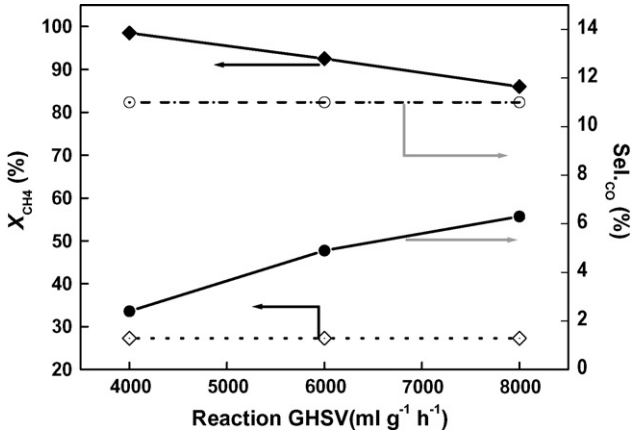

Fig. 10. Influences of reaction gas hourly space velocity on methane conversion and CO selectivity in membrane reactor (◆, experimental methane conversion; ◇, equilibrium methane conversion; ●, experimental CO selectivity; ○, equilibrium CO selectivity, working conditions, $T = 823$ K, $P = 900$ kPa, S/C = 3.0 and $I = 2.6$).

3.4.4. Influences of steam-to-carbon feed ratio

MSR reaction was carried out above a stoichiometric S/C to avoid carbon deposition over catalysts usually, which also enhance the steam reforming forward reactions. In CFBR, S/C of 3.0–4.0 is usually applied. While in membrane reactor, on one hand, lower reaction temperature would promise a lower S/C for carbon deposition suppression; on the other hand, due to the selective removal of H_2 by Pd membrane and high selectivity to CO_2, S/C higher than 2.0 are necessary. So, S/C for MSR reaction in membrane reactor was usually kept within 2.0–4.0. The effects of S/C ratio on methane conversion and CO selectivity obtained at $T = 823$ K, $P = 500$ kPa and GHSV of methane = 1000 mL g_{cat}^{-1} h^{-1} are shown in Fig. 11. The methane conversion in CFBR increases monotonically with increasing S/C. In this work, the same trend was also observed. Increase in S/C from 2.5 to 3.5 led to methane conversion increment from 93.8 to 99.0% in the membrane reactor. But the H_2 recovery rate does not change monotonically with increasing S/C. Actually, a decrease of recovery from 97.5% to about 94% was found in our experimental conditions when the S/C was increased from 2.5 to 3.5. Lower CO selectivity was also observed at a higher S/C. At S/C of 2.5, the CO selectivity was 6.5% while thermodynamic control one was 11.8%; at S/C of 3.5, the corresponding values were 2.4% and 10.5%, respectively. However, maximum H_2 yield was found at S/C = 3.0 in the investigated conditions. The results suggested that too large an excess of steam dilutes the H2 in the products mixture, which results in a decrease of the H2 partial pressure drop across the membrane and thus in a lower recovery rate of hydrogen. For instance, increase in S/C ratio from 2.5 to 3.5 resulted in recovery rate of hydrogen decrease from 97.0 to 94.0%. Shu et al. [13] gave a detailed investigation on the effects of S/C on methane conversion in Pd-based membrane reactors. The trend that higher S/C resulted in higher methane conversion at $T = 773$ K, $P = 136$ kPa, GHSV = 1067 h^{-1} and $I = 1.0$, was also found. Calculation made by Jogensen et al. [22] showed that by keeping S/C higher than 2.5, it was possible to avoid carbon deposition, even if H_2 was removed from reaction at 773 K. So, in our work, S/C was kept around 3.0 and no carbon deposition was found during reaction.

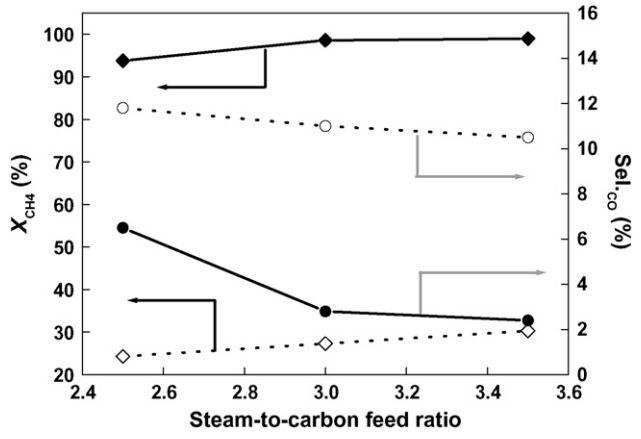

Fig. 11. Influence of steam-to-carbon feed ratio on methane conversion and CO selectivity in membrane reactor (◆, experimental methane conversion; ◇, equilibrium methane conversion; ●, experimental CO selectivity; ○, equilibrium CO selectivity, working conditions: $T = 823$ K, $P = 900$ kPa, GHSV of methane = 1000 mL g_{cat}^{-1} h^{-1} and $I = 2.6$).

3.4.5. Influence of sweep gas flux

A sweep gas is important to maintain a higher H_2 partial pressure drop across membrane to promote H_2 permeation and H_2 recovery rate, especially when reaction pressure is low. Generally, a higher sweep ratio promises a higher methane conversion [12,13]. The influences of sweep ratio on methane conversion and CO selectivity are indicated in Fig. 12. The reactions were carried out at $T = 823$ K, $P = 500$ kPa, GHSV = 6000 mL g_{cat}^{-1} h^{-1} and S/C = 3.0. Methane conversion was much lower when no sweep gas was used comparing to that using a low sweep ratio. For example, increase in methane conversion from 64.0 to 84.6% was obtained when the sweep ratio was increased from 0 to 1.7. However, increase in the sweep ratio from 1.7 to 3.4 only resulted in methane conversion increase from 84.6 to 89.8%. The effect of sweep ratio on CO selectivity was also small. The CO selectivity was 10.5% at $I = 0$, slightly lower than thermodynamic control one of 13.8%; while it was 7.6% at $I = 3.4$. The recovery rate of hydrogen also significantly increased from 57.5% at $I = 0$ to 80.9% at $I = 1.7$. However, further increase sweep ratio to $I = 2.6$ and $I = 3.4$ only lead to recovery rate of hydrogen of 82.7 and 85.2%, respectively. The fast leveling off of sweep gas influences on methane conversion and CO selectivity may be related with the sweep gas design mode. As previously reported [49], a countercurrent sweep gas design brought out an almost zero H_2 partial pressure at the position where membrane separation ended irrespective of sweep ratio. The leveling off of sweep ratio effect was also found in previous investigations [12,13]. Simulation models build by Oklany et al. [36] also predicted the same trend, too. The sweep gas design mode also had great influences on the H_2 partial pressure distributions in the permeate side along the axis of the Pd membrane. In a co-current sweep gas mode, the H_2 partial pressure in the reaction side first increases along the catalyst bed, then decreases when H_2 flux through Pd membrane was higher than H_2 production

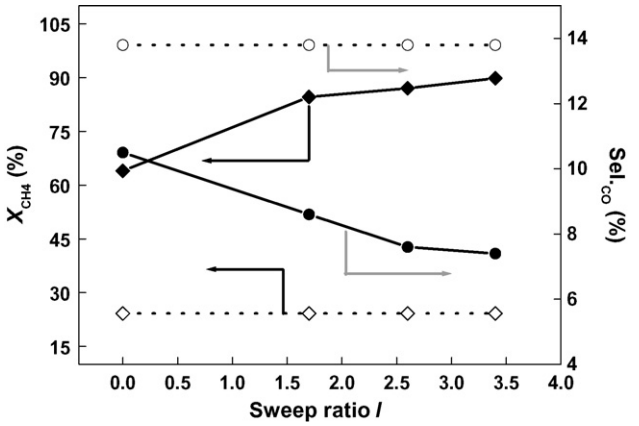

Fig. 12. Influences of sweep ratio on methane conversion and CO selectivity (◆, experimental methane conversion; ◇, equilibrium methane conversion; ●, experimental CO selectivity; ○, equilibrium CO selectivity, $T = 823$ K, $P = 500$ kPa, GHSV = 6000 mL g_{cat}^{-1} h^{-1} and S/C = 3.0).

Table 2
Methane conversion in Pd-based membrane reactor achieved in this work and comparison with some previous literature results

Membrane	Membrane properties	Operation conditions	X_{CH_4}(%)
Pd/PG[12]	ELP, δ = 20 μm A = 25.1 cm^2	T = 773 K, P = 100 kPa, Ni/Al_2O_3 13.0 g CH_4 25 mL min^{-1}, S/C = 3.0, SG (Ar) 400 mL min^{-1}	88
Pd/MPSS[12]	ELP, δ = 19.8 μm A = 10.7 cm^2	T = 773 K, P = 136 kPa, Ni/Al_2O_3 11.0 g CH_4 40 mL min^{-1}, S/C = 3.0, vacuum pumping	63
Pd-PdAg/MPSS[12]	ELP, δ = 10.3 μm A = 10.7 cm^2	T = 773 K, P = 136 kPa, Ni/Al_2O_3 13.0 g CH_4 40 mL min^{-1}, S/C = 3.0, SG (He) 40 mL min^{-1}	j51
Pd-Ag[13]	Cold rolling, δ = 50 μm, A = 46.1 cm^2	T = 723 K, P = 122 kPa, Ni/Al_2O_3 3.1 g CH_4 7.29–17.8 mL min^{-1}, S/C = 3.0, SG (O_2) = 400 mL min^{-1}	70
Pd-Ag[13]	Cold rolling, δ = 50 μm, A = 46.1 cm^2	T = 723 K, P = 122 kPa, Ni/Al_2O_3 3.1 g CH_4 7.29–17.8 mL min^{-1}, S/C = 3.0, SG (H_2O) = 400 mL min^{-1}	61
Pd/MPSS[14]	ELP, δ = 20–25 μm A = 70 cm^2	T = 773 K, P = 300–600 kPa, G56H GHSV 1600 L/(kg h), S/C = 3.0, SG = 0 mL min^{-1}	∼45
Pd/porous Inconel disk[15]	ELP, δ = 70–100 μm A = 70 cm^2	T = 1,023 K, P = 2,200 kPa, Ni/Al_2O_3 S/C = 2.2, SG = 0 mL min^{-1}	55
Pd-Ag/Al_2O_3[16]	ELP, δ = 5.2–22.5 μm, A = 12.6 cm^2	T = 773 K, P = 100 kPa, Ni/Al_2O_3 GHSV = 672 L (kg h)$^{-1}$	60–80
Pd/MPSS[25]	MDELP, δ = 6 μm A = 20 cm^2	T = 723 K, P = 300 kPa, Ni/Al_2O_3 15 g CH_4 25 mL min^{-1}, S/C = 3.0, SG = 500 mL min^{-1}	84
Pd/MPSS[25]	MDELP, δ = 6 μm A = 20 cm^2	T = 773 K, P = 300 kPa, Ni/Al_2O_3 15 g CH_4 25 mL min^{-1}, S/C = 3.0, SG = 500 mL min^{-1}	98
Pd/MPSS[25]	MDELP, δ = 6 μm A = 20 cm^2	T = 823 K, P = 500 kPa, Ni/Al_2O_3 15 g CH_4 50 mL min^{-1}, S/C = 3.0, SG = 500 mL min^{-1}	97
This work	MELP, δ = 4 μm A = 15.7 cm^2	T = 723 K, P = 900 kPa, Ni-La/Mg-Al 5.0 g GHSV = 4000 L (kg h)$^{-1}$, S/C = 3.0, SG = 220 mL min^{-1}	64.8
This work	MELP, δ = 4 μm A = 15.7 cm^2	T = 773 K, P = 900 kPa, Ni-La/Mg-Al 5.0 g GHSV = 4000 L (kg h)$^{-1}$, S/C = 3.0, SG = 220 mL min^{-1}	91.1
This work	MELP, δ = 4 μm A = 15.7 cm^2	T = 823 K, P = 900 kPa, Ni-La/Mg-Al 5.0 g GHSV = 4000 L (kg h)$^{-1}$, S/C = 3.0, SG = 220 mL min^{-1}	98.8
This work	MELP, δ = 4 μm A = 15.7 cm^2	T = 823 K, P = 900 kPa, Ni-La/Mg-Al 5.0 g GHSV = 4500 L (kg h)$^{-1}$, S/C = 3.5, SG = 220 mL min^{-1}	99.0

ELP: electroless plating, MPSS: macroporous stainless steel, PG: porous glass, MDLEP: multi-dimension electroless plating, MELP: modified electroless plating.

rate. While in the permeate side, H_2 partial pressure increases along the axis of the Pd membrane due to the accumulation of H_2 along the axis of the membrane. As the permeance of the Pd membrane was sufficiently high, the driving force for H_2 permeation at the position where the separation ended was supposed to greatly affect the separation efficiency of the Pd membrane. Co-current sweep gas would result in a higher H_2 partial pressure at the position where membrane separation ended than a countercurrent sweep in the permeate side. So, a higher separation efficiency and H_2 recovery rate could be expected, when a countercurrent sweep gas was designed, instead of a concurrent sweep gas. The high H_2 recovery, high separation efficiency of the Pd membrane was attributed to the combination the high permeance Pd membrane with the sweep gas operated in a countercurrent mode.

To sum up, the performances of Pd membrane reactor are closely related to the performance of Pd membrane, catalyst applied, working conditions and special design of membrane reactor configuration. Results achieved in thus work are compared with previous investigations in terms of methane conversion, as shown in Table 2. From the table, it has been clearly demonstrated that almost complete methane conversion could be achieved under mild working conditions. This process may find its application to on-site hydrogen production for application to proton exchange membrane fuel cells, using the widely available natural gas infrastructure.

4. Conclusions

High performance Pd composite membrane was successfully developed via a novel electroless plating method and applied to construct a membrane reactor for methane steam reforming (MSR) reaction at lower reaction temperatures. In contrast with most previous investigations, nickel-based catalyst prepared by coprecipitation–deposition and pre-reduced at higher temperature was applied for MSR in the membrane reactor, which also showed high activity for MSR at low reaction temperatures in conventional fixed bed reactor. The high activity may be ascribed to the formation of spinel structure during calcination, after reduction, it was supposed

that nickel species was well segregated and even monodispersed, which needs further confirmation. The combination of highly active MSR catalyst, high permeance Pd membrane and a countercurrent sweep gas design resulted in a much better results than those previously reported, a H_2 yield of 3.74 was achieved under optimized, mild working conditions. Not only methane conversion much higher than thermodynamic control ones but also CO selectivity much lower than thermodynamic control values were achieved in this work. As the permeance of the Pd membrane was high and the kinetics of catalyst fast, the performance of the membrane reactor may be determined by radial diffusion or concentration polarizations. So, in the modeling and simulation works, as well as in a practical membrane reactor, these influences could not be ignored. Currently, great effort is focused on the process durability aspects.

Acknowledgements

The authors are grateful to the natural basic research program of China (No. 2005cb221401), to the assistance of Professor Y. Chen and C. Yu, Dr. K. Jiang, L. Yuan in the Pd composite membrane preparation and to the helpful discussion with Dr. Q. Ge.

References

[1] J.P. Breen, R. Burch, H.M. Coleman, Appl. Catal. B: Environ. 39 (2002) 65.
[2] T. Davidian, N. Guilhaume, E. Iojoiu, H. Provendier, C. Mirodatos, Appl. Catal. B: Environ. 73 (2007) 116.
[3] Y. Chen, H. Xu, Y. Wang, X. Jin, G. Xiong, Fuel Process. Technol. 87 (2006) 971–978.
[4] M. Watanabe, H. Yamashita, X. Chen, J. Yamanaka, M. Kotobuki, H. Suzuki, H. Uchida, Appl. Catal. B: Environ. 73 (2007) 237.
[5] T. Tabakova, V. Idakiev, K. Tenchev, F. Boccuzzi, M. Manzoli, A. Chiorino, Appl. Catal. B: Environ. 63 (2006) 94.
[6] A. Lindermeir, S. Kah, S. Kavurucu, M. Mŭhlner, Appl. Catal. B: Environ. 70 (2007) 488.
[7] R.D. Cortright, R.R. Davda, J.A. Dumesic, Nature 418 (2002) 964.
[8] G.W. Huber, J.W. Shabaker, S.T. Evans, A. James, Dumesic, Appl. Catal. B: Environ. 62 (2006) 226.
[9] K. Murata, M. Saito, M. Inaba, I. Takahara, Appl. Catal. B: Environ. 70 (2007) 509.
[10] T. Giroux, S. Hwang, Y. Liu, W. Ruettinger, L. Shore, Appl. Catal. B: Environ. 56 (2005) 95.
[11] D.K. Lee, I.H. Baek, W.L. Yoon, Chem. Eng. Sci. 59 (2004) 931.
[12] S. Uemiya, N. Sato, H. Ando, T. Matsuda, E. Kikuchi, Appl. Catal. 67 (1991) 223.
[13] J. Shu, B.P.A. Grandjean, S. Kaliaguine, Appl. Catal. A 119 (1994) 305.
[14] K.I. Prokopiev, Y.I. Aristov, V.N. Parmon, N. Giordano, Int. J. Hydrogen Energy 17 (1992) 275.
[15] E. Kikuchi, Catal. Today 56 (2000) 97.
[16] J. Tong, Y. Matsumura, Appl. Catal. A 286 (2005) 226.
[17] E. Kikuchi, Y. Nemoto, M. Kajiwara, S. Uemiya, T. Kojima, Catal. Today 56 (2000) 75.
[18] M. Oertel, J. Schmitz, W. Weirich, D. Jendryssek-Neumann, R. Schulten, Chem. Eng. Technol. 10 (1987) 248.
[19] S. Uemiya, Y. Kude, K. Sugino, N. Sato, T. Matsuda, E. Kicuchi, Chem. Lett. 17 (1988) 1687.
[20] S. Uemiya, N. Sato, H. Ando, Y. Kude, T. Matsuda, E. Kikuchi, J. Membr. Sci. 56 (1991) 303.
[21] X. Pan, G.X. Xiong, S.S. Sheng, N. Stroh, H. Brunner, Chem. Commun. (2001) 2536.
[22] S.L. Jorgensen, P.E.H. Nielson, P. Lehrmann, Catal. Today 25 (1995) 303.
[23] Y. Lin, S. Liu, C. Chuang, Y. Chu, Catal. Today 82 (2003) 127.
[24] F. Gallucci, L. Paturzo, A. Fama, A. Basile, Ind. Eng. Chem. Res. 43 (2004) 928.
[25] J. Tong, Y. Matsumura, H. Suda, K. Haraya, Ind. Eng. Chem. Res. 44 (2005) 1454.
[26] Y. Matsumura, T. Nakamori, Appl. Catal. A 258 (2004) 107.
[27] K. Kusakabe, K. Sotowa, T. Eda, Y. Iwamoto, Fuel Process. Technol. 86 (2004) 319.
[28] P.F. Aparicio, M. Benito, K. Kouachi, S. Menad, J. Catal. 231 (2005) 345.
[29] D.C. Kruissink, L.L. Van Reijen, J.R.H. Ross, J. Chem. Soc., Faraday Trans. 1 77 (1981) 649.
[30] L.E. Alzamora, J.R.H. Ross, D.C. Kruissink, J. Chem. Soc., Faraday Trans. 1 77 (1981) 665.
[31] L. Garcia, A. Benedicto, R. Bilbao, et al. Energy Fuels 16 (2002) 1222.
[32] J.R.H. Ross, M.C.F. Steel, A. Zeini-Isfahani, J. Catal 52 (1978) 280.
[33] Y. Chen, H. Xu, X. Jin, G. Xiong, Catal. Today 116 (2006) 334.
[34] B. Vos, E. Poels, A. Bliek, J. Catal. 198 (2001) 77.
[35] G. Barbieri, V. Violante, F.P.D. Miao, A. Criscuoli, E. Drioli, Ind. Eng. Chem. Res. 36 (1997) 3369.
[36] J.S. Oklany, K. Hou, R. Hughes, Appl. Catal. A 170 (1998) 13.
[37] G. Barbieri, G. Marigliano, G. Perri, E. Drioli, Ind. Eng. Chem. Res. 40 (2001) 2017.
[38] F. Gallucci, L. Paturzo, A. Fama, A. Basile, Int. J. Hydrogen Energy 29 (2004) 611.
[39] Y. Chen, Y. Wang, H. Xu, G. Xiong, Ind. Eng. Chem. Res. 46 (2007) 5510.
[40] R. Martínez, E. Romero, C. Guimon, R. Bilbao, Appl. Catal. A 274 (2004) 139.
[41] J. Sloczynski, J. Ziolkowski, B. Grzybowska, et al. J. Catal. 187 (1999) 410.
[42] D.N. Bangala, N. Abatzoglou, E. Chornet, AIChE J. 44 (1998) 927.
[43] S.D. Robertson, B.D. Mc Nicol, H. De Bass, S.C. Kloet, J.W. Jenkins, J. Catal. 37 (1975) 424.
[44] A.C.S.C. Teixeira, R. Giudici, Chem. Eng. Sci. 54 (1999) 3609.
[45] A. Li, W. Liang, R. Hughes, J. Membr. Sci. 149 (1998) 259.
[46] P. Mardilovich, Y. She, Y. Ma, M. Rei, AIChE J. 44 (1998) 310.
[47] R. Dittmeyer, V. Hllein, K. Daub, J. Mol. Catal. A: Chem. 173 (2001) 135.
[48] G. Xomeritakis, Y. Lin, J. Membr. Sci. 120 (1996) 261.
[49] Y. Chen, H. Xu, Y. Wang, G. Xiong, Catal. Today 118 (2006) 136.
[50] N. Itoh, W. Xu, K. Haraya, Ind. Eng. Chem. Res. 33 (1994) 197.
[51] G. He, Y. Mi, P.L. Yue, G. Chen, J. Membr. Sci. 153 (1999) 243.